Applied Energy 247 (2019) 309–321

Contents lists available at ScienceDirect

Applied Energy

journal homepage: www.elsevier.com/locate/apenergy

Modeling and field-test of a compact electromagnetic energy harvester for railroad transportation

Yu Pan[a], Teng Lin[b], Feng Qian[a], Cheng Liu[c], Jie Yu[c], Jianyong Zuo[c], Lei Zuo[a,*]

[a] Center for Energy Harvesting Materials and Systems (CEHMS), Virginia Tech, Blacksburg, VA 24061, USA
[b] Department of Mechanical Engineering, Stony Brook University, Stony Brook, NY 11790, USA
[c] Institute of Rail Transit, Tongji University, Shanghai 201804, China

HIGHLIGHTS

- A compact ball screw based design reduces the backlash in the motion transmission.
- A coupled model is developed to predict the energy harvesting performance.
- Lab tests are conducted to evaluate harvester and validate the model.
- Filed tests prove the performance of the harvester under the real condition.

ARTICLE INFO

Keywords:
Railway energy harvesting
Mechanical motion rectifier
Ball screw
Railway track dynamics

ABSTRACT

To enable the smart technologies and safe operation of transit and rail transportation, such as hot box detector, track health monitoring and wireless communication on the railroad side, a cost-effective energy source is in need. This paper presents the design, modeling, in-lab experiment and field-test results of a compact ball-screw based electromagnetic energy harvester with a mechanical motion rectifier (MMR) mechanism for smart railway transportation. The MMR mechanism is realized by the embedded one-way clutches in the bevel gears, which converts the bi-directional track vibration into the unidirectional rotation of the generator. Compared to previous designs, the proposed harvester has reduced backlash and thus can harvest energy from a small input of the track deflection induced by the moving train. Two prototypes with different key design parameters were built and tested. A comprehensive model considering the train-rail-harvester interaction was developed to analyze the dynamic characteristics of the coupled system and predict the energy harvesting performance of the harvesters at different train speeds. Both in-lab and field tests were carried out to examine the energy harvesting performance of the harvesters and validate the model. Field test results illustrated that an average power of 1.12 W and 2.24 W were achieved for two prototypes respectively when a Type A rapid transit passed by with a 30 km/h vehicle speed.

1. Introduction

In the past decade, energy harvesting techniques which could be used for powering smart electronic devices have received increasing attention. Based on piezoelectric and electromagnetic method via linear and nonlinear [1,2] mechanism, researchers have investigated energy harvesting in many different modes including ocean waves [3,4], wind flow [5], vibrations in automobile suspension [6,7] and transportation infrastructure [8,9].

For transporting passengers living inner city, the rapid transit system has become one significant option in recent decades. Often seen along urban growth in congested cities, rapid transit systems are an appealing solution for reducing vehicle traffic. Interconnected metro lines cross, merge, and mingle with others beneath the crowded cities, leaving the safety consideration for the rapid transit system to be the first priority. To achieve a safe and reliable transportation operation, many trackside electrical devices or smart technologies, such as signal lights, track switches, hot box detectors, rail health monitoring systems, and wireless communication modules, have been applied to the rail system. Let alone the sophisticated operation auxiliaries, the tunnel lights themselves consume a lot of electricity. However, cost-effective stable power supplies for tunnel lights are very limited. Seeking an

* Corresponding author.
E-mail address: leizuo@vt.edu (L. Zuo).

https://doi.org/10.1016/j.apenergy.2019.03.051
Received 20 September 2018; Received in revised form 5 February 2019; Accepted 7 March 2019
Available online 17 April 2019

alternative cost-effective power source for the railway safety electrical devices has been an appealing research topic for the industry.

There is a vast energy potential in the railway track deflection induced by wheel-rail vertical contact force. The amplitude and frequency of railway track deflection can vary from 1 to 12 mm and 1–4 Hz, respectively, depending on the types of trains, track structures and carrying loads [10,11]. Aiming at utilizing a relatively small fraction of the energy stored in the railroad tracks to power the electronic safety devices, many energy harvesting technologies, such as those using piezoelectric [12–16], hydraulic [14,17] and electromagnetic [14,18–29], have been widely studied. For example, Wischke *et al.* [12] developed a piezoelectric vibration harvester equipped with a power interface circuit to power wireless sensor nodes in railway tunnels, and an average energy of 395 μJ per train was achieved during the in-field test. Nelson *et al.* [13] and Pourghodrat *et al.* [14] developed a piezoelectric energy harvester which can be mounted on the bottom of the rail track, exposing it to longitudinal strain during the passing of trains. Numerical simulation indicated a maximum average power output of 1.1 mW and an average power of 53 μW were obtained in the field test when an unloaded train traveled at approximately 24 km/h (15 mph). Yuan *et al.* [15] established a model of piezoelectric drum harvester with 100 mW in the simulation analysis. An experiment was conducted in lab using a 1:10 track test rig with a single wheel and an average 0.1 mW was achieved when the speed of the wheel ran at 0.5 km/h. Wang *et al.* [16] established a detailed model for a piezoelectric stack in the railway track model under moving multi-loads and an average power of 0.19 mW was obtained in the simulation. Overall, due to low power output and high impedance of piezoelectric material, the harvested power could only supply sensors for health monitoring purpose. This suggests that it is inadequate for most safety electronic devices such as signal lights, track switches, and hot box detectors. Hydraulic energy harvester for railway track has also been studied. *Pourghodrat, Nelson, and co-workers* [14,17] designed a hydraulic energy harvester with hydraulic motor, planetary gearbox, and a generator. An average power of 11 W was obtained in the lab bench test under 3.75 mm and 0.375 Hz harmonic excitation. However, there is no field test to validate its energy harvesting performance under real track vibrations.

Other than piezoelectric and hydraulic harvesters, mechanical based electromagnetic energy harvesters have been gaining more popularity in the past decade. Nelson *et al.* [13] and Pourghodrat *et al.* [14] designed an inductive voice coil energy harvester with the coil rigidly attached to the rail track and a permanent magnet with a radial magnetic field fixed on the ground. A maximum average power of 0.146 mW was derived under a low-amplitude, 10-Hz sinusoidal excitation in the lab bench test. However, field tests provided different results including an average power of 4 mW when a train consisting of empty cars traveled at 18 km/h (11 mph) and an average power of 12 mW when a loaded train ran at 21 km/h (13 mph). Gao *et al.* [18] also developed a linear electromagnetic energy harvester with an inductive coil and an average power of 119 mW was attained with a simulated rail displacement of 1.2 mm in the lab bench test. Gatti et al. [19] researched on harvesting energy from the vibration of a passing train using a single-degree-of-freedom mechanical oscillator, and the amount of energy harvested per unit mass is found to be proportional to the product of the square of the input duration and acceleration amplitude. Brennan *et al.* [20] presented an investigation about the upper bound of the scavenged energy on mechanical oscillators, which can be used for harvesting energy from track deflections, and conducted a fundamental study to determine the optimal set of mechanical design parameters of a linear single degree of freedom spring-mass-damper system.

Besides linear electromagnetic harvesters, many researchers have designed rotary harvesters which could have a higher power density than linear harvesters and can convert the bi-directional track vibration into rotation of an electromagnetic generator. Pourghodrat *et al.* [14,21,22] proposed a mechanical energy harvester using rack and pinion mechanism with a clutch bearing to harvest the track vibration energy when the track moves down, while generator freewheels when the track moves up. The in-field test results showed an average power of 0.22 W was obtained with 12.7 mm (0.5 in) track deflection when a loaded train traveled at 18.5 km/h (11.5 mph). They also provided another updated design, which can harvest energy when the track vibrates in both directions, and simulation results showed a significant improvement in performance. Wang *et al.* [23] proposed a design to convert the bi-directional vibration into uni-directional rotation by using three shafts, three spur gears, a pair of rack and pinion, and two roller clutches. Lab test results indicated a maximum average power of 1.4 W was obtained with a 10–25% mechanical efficiency. Much of its low efficiency was attributed to the design complexity and backlash between the rack and pinion gears. Zhang *et al.* [24,25] proposed two different kinds of track energy harvester design and lab tests illustrated that a 55.5% mechanical efficiency and a peak voltage of 58 V at 1 Hz with a displacement of 2.5 mm were achieved, respectively. Wang and Lin *et al.* [26,27] proposed a simplified single shaft rack-pinion design and then Lin *et al.* [28,29] implemented an anchorless mounting in an updated design using MMR, converting the bi-directional track vibration into unidirectional rotation of the generator and increasing the energy harvesting performance. The single shaft design achieved a 74% mechanical efficiency [27] because of less friction loss, and the anchorless prototype [28,29], with 60 cm length, 15 cm height and 40 kg weight, can be installed in-field without any physical anchor, avoiding damages to the railroad subgrade. An average power of 6.9 W was obtained by the anchorless prototype under a 5.7 mm freight train track deflection infield when the train traveled at 64 km/h (40 mph).

Overall, among the energy harvesting technologies, the rack pinion based electromagnetic energy harvesters, especially those with MMR mechanism, have proven to have reasonable performance for powering trackside electronics. However, three main challenges remain in the existing technologies: (i) almost all the current rotary track energy harvesters are relatively cumbersome or not easy to install; (ii) the backlash between the rack teeth and pinion teeth in rack-pinion based harvesters can be large and lead to relatively low energy harvesting performance when the excitation is small [30,31]; (iii) a coupled model consists of the train, harvester and track system is needed for predicting the energy harvesting performance at different train speeds.

In this paper, a compact design with an MMR mechanism is proposed for harvesting energy from rapid transit track deflection in the tunnels or freight track deflection. The energy could be stored in a battery through self-designed or commercial battery charging circuits and used to power different trackside electrical devices, such as signal lights, track switches, hot box detectors, rail health monitoring systems, and wireless communication modules, which could potentially increase the safety of train operation. Two prototypes are fabricated using the ball screw mechanism with less backlash during transmission and high sensitivity to the vibration environment. A systematic model considering the train-track-harvester interaction is developed to analyze the dynamic characteristics of the coupled system and predict the energy harvesting performance of the harvesters at different train speeds. In-lab and field tests have been carried out to examine the performance of the harvester and validate the model. Field test results show that an average power of 1.12 W and 2.24 W are achieved for prototype 1 and 2 respectively at 30 km/h.

This paper is organized as follows. Section 2 introduces the detailed design and working principle of the two prototypes with different parameters. Section 3 is the systematic modeling for the proposed energy harvester coupled with the rail system. Section 4 is the in-lab test of the proposed energy harvesters and Section 5 is the harvester in-filed test. Section 6 provides the concluding remarks.

2. Design and working principle

The proposed track energy harvester is comprised of a ball screw, an

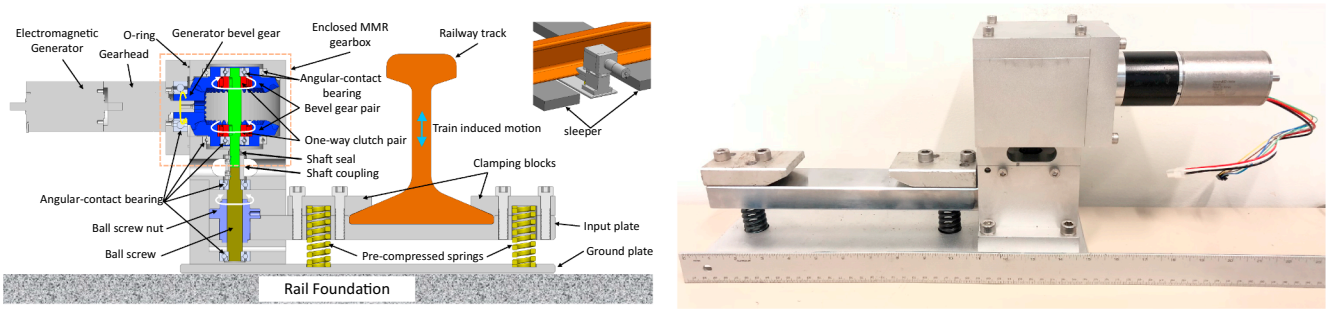

Fig. 1. Design of the ball screw based railway track energy harvester with MMR mechanism: (a) Design details (b) Prototype.

enclosed MMR gearbox, an electromagnetic generator with a gearhead and anchorless mounting parts, as shown in Fig. 1(a). Compared with previous rack pinion based designs [27,29], the ball screw mechanism can significantly reduce the backlash during the process of converting the bi-directional linear motion to rotation [31]. Therefore, it can provide a higher energy harvesting performance when the excitation displacement is small. The harvester is designed to be installed under the track between two adjacent sleepers, and the input plate could be considered as rigidly connected with the railway track by two clamping blocks with bolts. The bending stiffness of the input plate (made of steel) is large enough so that the deformation of the input plate can be ignored. In order to quickly install the harvester on site and prevent the potential risk of the physical anchor from changing the property of ballast and subgrade, two reset springs are pre-loaded and positioned between the input plate and ground plate, providing enough spring force to keep the ground plate stationary on the rail foundation. When the train passes by, the track deflects due to the wheel-rail vertical contact forces and the input plate of the harvester vibrates together with the track vertically. The ball nut is embedded near one end of the input plate and the ball screw is used in the back-driven mode, which can convert the low speed reciprocal linear motion of the track vibrations into bi-directional rotation of the screw at a higher speed. A mechanical coupler is employed to connect the screw shaft and the input shaft of the enclosed MMR gearbox so that the input shaft can also rotate bi-directionally.

The enclosed MMR gearbox consists of a pair of large bevel gears embedded with one-way sprag clutches, a small bevel gear connected with the gearhead shaft and five angular contact bearings. The rotational motion could be transmitted from the large bevel gear pair to the small bevel gear, and consequently, the gearhead and electromagnetic generator could rotate as well. Angular contact bearings are applied to provide shaft and gears with both the radial and thrust forces so that the overall transmission could be smooth and steady. Meanwhile, shaft seals and o-rings are used in the gearbox design, so, by adding the lubricant oil or grease inside the enclosed gearbox, the transmission reliability and efficiency could be improved.

Fig. 2 illustrates the working principle of the ball screw based MMR railway track energy harvester. For instance, in Fig. 2, if the track moves down when the train wheel approaches, the ball screw will spin counter-clockwise from the bottom view, and at this moment, the upper bevel gear can be engaged with the embedded clutch and become the driving gear, while the lower bevel gear is disengaged with the embedded clutch and becomes an idle gear. In this way, the small bevel gear is driven by the upper driving gear and will spin counter-clockwise (from the left view). If the track moves up when the train wheels move away, the ball screw will spin clockwise from the bottom view, and at this moment, the lower bevel gear is engaged with the embedded clutch and becomes the driving gear, while the upper bevel gear is disengaged from the embedded clutch and becomes an idle gear. In this way, the small bevel gear and thus the generator will continuously spin counter-clockwise (from the left view). In other words, no matter if the railway track moves upwards or downwards, the electromagnetic generator always rotates uni-directionally, resulting in high energy harvesting performance and low impact force during transmission [27]. This special mechanism, converting the reciprocating vibration into unidirectional rotation of the generator, is referred to as mechanical motion rectifier (MMR) [32]. Two prototypes are fabricated with the same design but different ball screw leads, reset springs, gearheads, and generators. The main parameters of these two prototypes are listed in Table 1.

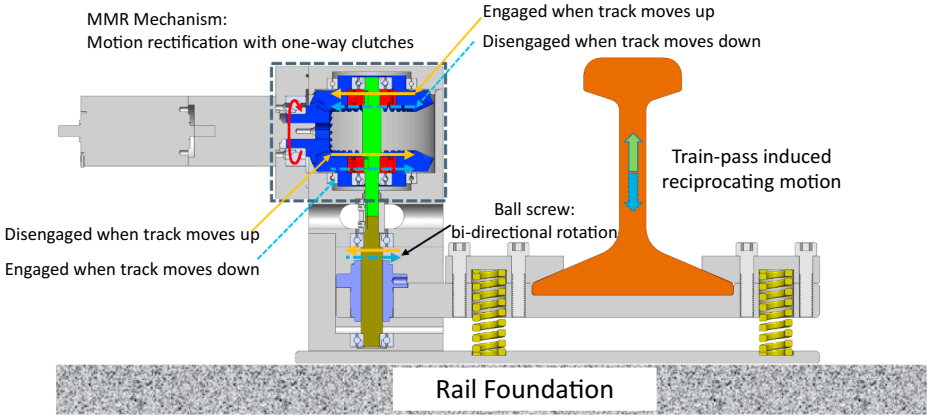

Fig. 2. Bidirectional vertical track motion induced by wheel-rail vertical contact force will drive the generator to rotate in one direction using the proposed ball screw MMR mechanism: green lines represent the case that track moves up and blue lines represent the case that the track moves down.

Table 1
Parameters of the proposed energy harvesters.

Parameters	Value	Description	Parameters	Value	Description
d_m	15.75 mm	Screw diameter	r_b	2	Bevel gear transmission ratio
l_1	20 mm	Screw lead in Prototype 1	r_{1g}	4.3	Generator 1 gearhead ratio
l_2	16 mm	Screw lead in Prototype 2	r_{2g}	12	Generator 2 gearhead ratio
J_{1m}	3.06 kg cm^2	Generator inertia of Prototype 1	k_{1e}	0.163 V/rads	Generator 1 voltage constant
J_{2m}	0.17 kg cm^2	Generator inertia of Prototype 2	k_{2e}	0.054 V/rads	Generator 2 voltage constant
J_{lg}	30 kg cm^2	Large gear inertia	k_{1t}	0.163 Nm/A	Generator 1 torque constant
J_{sg}	3 kg cm^2	Small gear inertia	k_{2t}	0.054 Nm/A	Generator 2 torque constant
J_{bs}	0.038 kg cm^2	Screw inertia	L_1	2.5 mH	Generator 1 phase to phase inductance
R_{1i}	2.28 Ω	Terminal resistance phase to phase of Generator 1	L_2	0.443 mH	Generator 2 phase to phase inductance
R_{2i}	0.284 Ω	Terminal resistance phase to phase of Generator 2	k_1	26269 N/m	Spring constant of Prototype 1
Stroke	15 mm	Harvester stroke	k_2	95269 N/m	Spring constant of Prototype 2
Weight	15 kg	Harvester weight	*Height*	20 cm	Harvester overall height

Note: Generator 1 and Generator 2 represent the generator inside the harvester prototype 1 and harvester prototype 2, respectively.

3. Modeling and system dynamics

3.1. Dynamics of the three-phase AC generator

A three-phase AC generator is applied in the proposed railway track energy harvester and a star shape tunable resistive load is employed in the energy harvesting circuit model. Fig. 3 shows the dynamic model of the three-phase AC generator.V_1, V_2, V_3 are the back electromotive force (EMF) of the generator, and i_1, i_2, i_3 are induced currents in each phase, respectively. L is the inductance of coils per phase, which has a negligibly small value, and R_i, R_e are internal and external resistance, respectively.

The dynamics and the electrical damping characteristics of the generator have been analyzed in [29]. By ignoring the inductance, the resistive torque T_{ge} induced by the electrical damping of the three-phase generator can be expressed as

$$T_{ge} = \frac{3k_t k_e}{2(R_i + R_e)}\omega_{ge} \tag{1}$$

where k_t and k_e are the speed and torque constants, and ω_{ge} is the angular velocity of the three-phase AC generator.

According to Newton's second law, the equation of motion of the generator can be expressed as

$$T_m - T_{ge} = J_m \dot{\omega}_{ge} \tag{2}$$

where T_m is the input torque. Substituting (1) into (2), the driving torque T_m for the generator can be written as

$$T_m = J_m \dot{\omega}_{ge} + \frac{3k_t k_e}{2(R_i + R_e)}\omega_{ge} \tag{3}$$

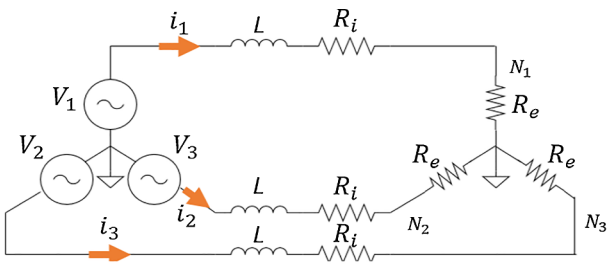

Fig. 3. Modeling of star shape three-phase generator with star shape resistive load [29].

3.2. Dynamic model of the proposed ball screw based track energy harvester

Fig. 4 illustrates the dynamic model of the proposed ball screw based energy harvester for railway track. Different from the linear harvesters and some rotary harvesters, ball screw based MMR harvester can convert the bi-directional linear vibration into the unidirectional rotation of generator by utilizing the one-way clutches embedded in the large bevel gears, producing nonlinear dynamic characteristics within the harvester. Specifically, when the ball screw angular velocity equals that of one of the large bevel gear, the one-way clutch embedded in that bevel gear is engaged to the shaft, so that the torque could be transmitted from the input shaft to the bevel gears and the generator is driven by small bevel gears to rotate. Instead, when the ball screw angular velocity is smaller than that of the large bevel gears, both one-way clutches embedded in the bevel gears are disengaged from the shaft, indicating that there is no motion transmission from the shaft to the bevel gears so that gears and generator will rotate freely due to their inertia.

Assuming the track deflection is x, velocity is $\dot{x}$, the ball screw lead is l , the gear ratio of the gearbox and MMR gearbox together is n_g, the rotational speed of the generator ω_{ge} at engagement period can be obtained as

$$\omega_{ge} = \frac{2\pi n_g}{l}\dot{x} \tag{4}$$

The resisting force on the ball screw nut due to the electrical damping of the generator, which can be obtained as

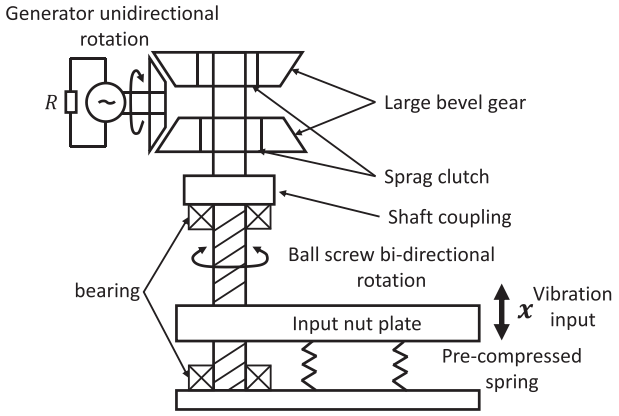

Fig. 4. Dynamic model of the proposed railway track energy harvester.

$$F_{damping} = \frac{2\pi n_g}{l} T_{ge} = \frac{6\pi^2 {n_g}^2 k_t k_e}{l^2 (R_i + R_e)} \dot{x} = c_e \dot{x} \tag{5}$$

where $c_e = \frac{6\pi^2 {n_g}^2 k_t k_e}{l^2 (R_i + R_e)}$, which can be regarded as the equivalent damping coefficient of the proposed energy harvester during the engagement period.

Using the energy method, the kinetic energy of the system could be obtained as follows

$$\sum_1^n T_{kinetic} = \frac{1}{2} m_e \dot{x}^2 \tag{6}$$

$$\sum_1^n T_{kinetic} = \frac{1}{2} m_{ip} \dot{x}^2 + \frac{1}{2} J_{bs} \omega_{bs}^2 + \frac{1}{2} J_s \omega_s^2 + \frac{1}{2} J_{lb} \omega_{lb}^2 + \frac{1}{2} J_{sb} \omega_{sb}^2 + \frac{1}{2} J_{gh} \omega_{gh}^2 + \frac{1}{2} J_{ge} \omega_{ge}^2 \tag{7}$$

$$\omega_{bs} = \omega_s = \omega_{lb} = 2\pi \frac{\dot{x}}{l} \tag{8}$$

$$\omega_{sb} = 2\omega_{lb} \tag{9}$$

$$\omega_{gh} = \omega_{ge} = 2\pi n_g \frac{\dot{x}}{l} \tag{10}$$

where m_e and $T_{kinetic}$ represent the equivalent mass and the kinetic energy of the engaged system, ω_{bs}, ω_s, ω_{lb}, ω_{sb}, ω_{gh}, andω_{ge} are the angular velocity of the ball screw, shaft, large bevel gear, small bevel gear, gearhead, and the generator respectively. J_{bs}, J_s, J_{lb}, J_{sb}, J_{gh}, andJ_{ge} represent the moment of inertia of the ball screw, shaft, large bevel gear, small bevel gear, gearhead, and the generator, respectively. m_{ip} is the mass of the input plate.

Substitute (7)–(10) into (6), the equivalent mass of the engaged system can be derived as

$$m_e = m_{ip} + \frac{4\pi^2}{l^2}(J_{bs} + J_{bs} + J_{lb} + 4J_{sb}) + \frac{4\pi^2}{l^2} {n_g}^2 J_{ge} \approx \frac{4\pi^2}{l^2} {n_g}^2 J_{ge} \tag{11}$$

In Eq. (11), the contribution of the inertia of the input plate, the gears, and the screws, $m_{ip} + \frac{4\pi^2}{l^2}(J_{bs} + J_{bs} + J_{lb} + 4J_{sb})$, is much smaller than that of the generator $\frac{4\pi^2}{l^2} {n_g}^2 J_{ge}$, especially when the gear amplification ratio is large. Therefore, the equivalent inertance of the proposed track energy harvester is mainly dominated by the rotational inertia of the electromagnetic generator. The inertia of other mechanical components could be negligible.

Hence, during the engagement period, the dynamic model of the proposed energy harvester can be simplified as a single degree of freedom spring-mass-damper system under a force excitation from the railway track. The total force the energy harvester gives to the railway track can be expressed as

$$F_{engage} = m_e \ddot{x} + c_e \dot{x} + 2k(x + \delta_0) = \frac{4\pi^2}{l^2} {n_g}^2 J_{ge} \ddot{x} + \frac{6\pi^2 {n_g}^2 k_t k_e}{l^2 (R_i + R_e)} \dot{x} + 2k(x + \delta_0) \tag{12}$$

where δ_0 is the original compression length of the pre-loaded springs. The above equation indicates that the energy harvester could be regarded as a fixed inerter in parallel with two pre-loaded springs and a tunable damper.

During the disengagement, the bevel gear disengages with the shaft, and therefore, there is no transmission from the shaft to the bevel gears. The only force from the energy harvester to the railway track is the spring force coming from the two reset springs, and at this time, the generator will rotate freely only with viscous damping from the generator.

In summary, the dynamics equation and the induced single-phase voltage of the proposed railway energy harvester could be obtained as

$$\begin{cases} F_{engage} = \frac{4\pi^2}{l^2} {n_g}^2 J_{ge} \ddot{x} + \frac{6\pi^2 {n_g}^2 k_t k_e}{l^2 (R_i + R_e)} \dot{x} + 2k(x + \delta_0) & Engagement \\ F_{disengage} = 2k(x + \delta_0) & Disengagement \end{cases} \tag{13}$$

$$\begin{cases} V_{ge} = 2\pi k_e n_g \sin\left(\int_0^t \omega_e dt + \frac{2k}{3}\pi\right) \frac{\dot{x}}{l} & Engagement \\ V_{ge} = \dot{\theta}_s(t) = e^{-\frac{c_e}{m_e}(t - t_0)} \dot{\theta}_{s0} \sin\left(\int_0^t \omega_e dt + \frac{2k}{3}\pi\right) & Disengagement \end{cases} \tag{14}$$

where t_0 and $\dot{\theta}_{s0}$ are the time and angular velocity when disengagement occurs, and ω_e is the angular frequency of the induced voltage of the generator, which will be ω_{ge} multiplied by the total number of generator pole pairs. $k = 0, 1, 2$, representing the 1st, 2nd and 3rd phase of the generator.

3.3. System dynamics

To further understand the dynamic interaction among the train, rail and track harvester and to predict the energy harvesting performance at different train speeds, a comprehensive model is established and presented in Fig. 5. A two-unit rapid transit train model is employed with four wheelsets per train. The wheel-rail vertical contact forces behave as the force input to the track-harvester system and can be considered as moving loads $f_1 \sim f_8$ with vehicle speedV_0. It has been investigated that railway track can be modeled as a simply supported beam if the rail length is longer than 100 m [33]. Neglecting the shear deformation and rotational inertia of the railway track, a uniform Euler-Bernoulli beam of mass m_r per unit length and flexural rigidity EI, with individual sleepers supported beneath, is applied in this model. Rail pads are positioned between the rail and sleepers to provide stiffness and damping, and sleepers are supported by the ballast bed. The proposed energy harvester, which can be considered as a fixed inertia mass in parallel with a tunable damper and pre-loaded springs, is installed between two adjacent sleepers, as shown in the red dash box in Fig. 5.

The equation of motion of the railway track could be written as

$$EI \frac{\partial^4 Z_r}{\partial x^4}(x, t) + m_r \frac{\partial^2 Z_r}{\partial t^2}(x, t) = f(x, t) \tag{15}$$

where Z_r is the rail deflection (subscript r means rail) and $f(x, t)$ is the

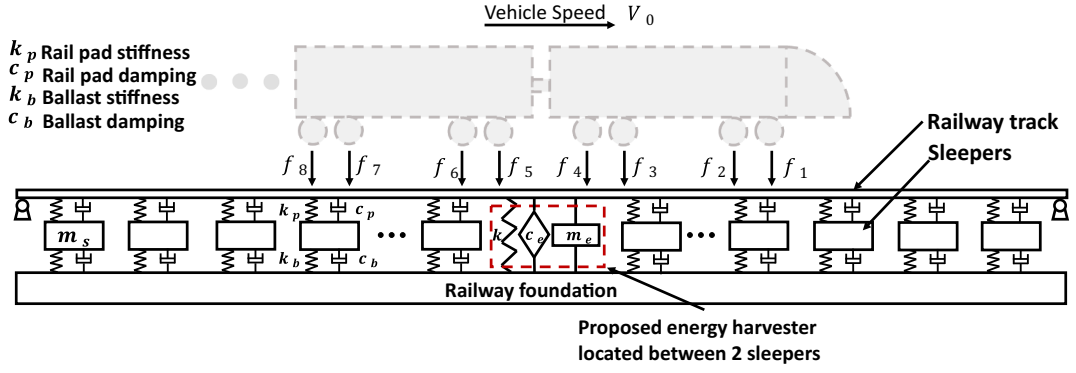

Fig. 5. Dynamic model of Train-track-harvester system.

total external forces applied on the rail, including the supporting forces $F_{rsk}(t)$ from the 1~ k sleepers (subscript rs means the force between the rail and sleeper, and k means the kth sleeper), eight wheel-rail vertical contact forces $P_l(t)$ (subscript l means the lth load) from the train wheels and supporting force $F_h(t)$from the proposed harvester (subscript h means the harvester). This three forces could be expressed as follows

$$F_{rsk}(t) = K_{pk}[Z_r(x_k, t) - Z_{sk}(t)] + C_{pk}[\dot{Z}_r(x_k, t) - \dot{Z}_{sk}(t)] \tag{16}$$

$$P_l(t) = f_0 \tag{17}$$

$$F_h(t) = \begin{cases} m_e\ddot{Z}_r(x_h, t) + c_e\dot{Z}_r(x_h, t) & Engagement \\ \quad + 2k_{spring}(Z_r(x_h, t) + \delta_0) & \\ 2k_{spring}(Z_r(x_h, t) + \delta_0) & Disengagement \end{cases} \tag{18}$$

where K_{pk}, C_{pk} are stiffness and damping of the rail pad; x_h, x_k are the horizontal coordinates of the harvester and kth sleeper; $Z_{sk}(t)$, $\dot{Z}_{sk}(t)$ are vertical displacement and velocity of kth sleeper; k_{spring} and δ_0 are the stiffness and pre-compressed length of the pre-loaded springs. The engagement happens when the rotational speed of one large bevel gear equals that of the input shaft, while the disengagement happens when the rotation of large bevel gears is larger than that of the input shaft and no torque transmission exists between the shaft and gears. The force $F_h(t)$ from the energy harvester is a piecewise linear function during engagement and disengagement, which endues the nonlinear characteristics to the system. The overall external force on the rail can be written as

$$f(x, t) = -\sum_{k=1}^{N} F_{rsk}(t)\delta(x - x_k) + \sum_{l=1}^{8} P_l(t)\delta(x - x_{wl}) - F_h(t)\delta(x - x_h) \tag{19}$$

where N is the number of sleepers, $\delta(x)$ is the Dirac delta function and x_{wl} (l = 1~ 8) is the horizontal coordinate of the eight moving loads.

By using the method of separation of variables, the deflection of the rail can be written as:

$$Z_r(x, t) = \sum_{i=1}^{M} \phi_i(x)q_i(t) \tag{20}$$

where $q_i(t)$ is the ith modal time coordinate and M is the total number of modes considered in the model. It has been investigated that a good convergence of the solution could be obtained if M is larger than half of the system degrees of freedom [33]. For simply supported Euler-Bernoulli beam, the mode shape function could be written as

$$\phi_i(x) = \sin\left(i\frac{\pi}{l}x\right) \tag{21}$$

For ith mode, the dynamic equation of the railway track is given by

$$EI\frac{\partial^4 Z_{ri}}{\partial x^4}(x, t) + m_r\frac{\partial^2 Z_{ri}}{\partial t^2}(x, t) = f(x, t) \tag{22}$$

After substituting Eq. (21) into (22) and performing some manipulation, we can get

$$EI\beta^4\phi_i(x)q_i(t) + m_r\phi_i(x)\frac{\partial^2 q_i(t)}{\partial t^2} = f(x, t) \tag{23}$$

where $\beta^4 = \frac{\omega^2}{c^2} = \frac{\rho A\omega^2}{EI}$. Using the orthogonality of the mode shapes, the above equation can be expressed as

$$EI\beta^4 q_i(t)\int_0^l \phi_i(x)\phi_j(x)dx + m_r\ddot{q}_i(t)\int_0^l \phi_i(x)\phi_j(x)dx = \int_0^l f(x, t)\phi_j(x)dx \tag{24}$$

where

$$\int_0^l \phi_i(x)\phi_j(x)dx = \begin{cases} 0 & i \neq j \\ \frac{l}{2} & i = j \end{cases} \tag{25}$$

Therefore, the final equation of motion for the rail is given by

$$EI\beta^4\frac{l}{2}q(t) + m_r\frac{l}{2}\ddot{q}(t) = \int_0^l f(x, t)\phi_i(x)dx \tag{26}$$

During the engagement period, the governing equation of the rail track could be expressed as

$$\left[m_r\frac{l}{2} + m_e\phi_i^2(x_h)\right]\ddot{q}_i(t) + \left[c_e\phi_i^2(x_h) + C_{pk}\sum_{k=1}^{N}\phi_i^2(x_k)\right]\dot{q}_i(t) - C_{pk}\sum_{k=1}^{N}\phi_i(x_k)\dot{Z}_{sk}(t) + \left[EI\beta^4\frac{l}{2} + 2k_{spring}\phi_i^2(x_h) + K_{pk}\sum_{k=1}^{N}\phi_i^2(x_k)\right]q_i(t) - K_{pk}\sum_{k=1}^{N}\phi_i(x_k)Z_{sk}(t) = \int_0^l\sum_{l=1}^{8}P_l(t)\delta(x - x_{wl})\phi_i(x)dx - \int_0^l 2k\delta_0\phi_i(x_h)\delta(x - x_h)dx \tag{27}$$

During the disengagement period, the governing equation of the rail track could be expressed as

$$m_r\frac{l}{2}\ddot{q}_i(t) + \left[C_p\sum_{k=1}^{N}\phi_i^2(x_k)\right]\dot{q}_i(t) - C_{pk}\sum_{k=1}^{N}\phi_i(x_k)\dot{Z}_{sk}(t) + \left[EI\beta^4\frac{l}{2} + 2k_{spring}\phi_i^2(x_h) + K_p\sum_{k=1}^{N}\phi_i^2(x_k)\right]q_i(t) - K_p\sum_{k=1}^{N}\phi_i(x_k)Z_{sk}(t) = \int_0^l\sum_{l=1}^{8}P_l(t)\delta(x - x_{wl})\phi_i(x)dx - \int_0^l 2k\delta_0\phi_i(x_h)\delta(x - x_h)dx \tag{28}$$

The equation of motion for the kth sleeper is given by

$$m_{sk}\ddot{Z}_{sk}(t) + (C_{pk} + C_{bk})\dot{Z}_{sk}(t) + (K_{pk} + K_{bk})Z_{sk}(t) - C_{pk}\sum_{i=1}^{N}\phi_i(x_k)\dot{q}_k(t) - K_{pk}\sum_{i=1}^{N}\phi_i(x_k)q_k(t) = 0 \tag{29}$$

where K_{bk}, C_{bk} are the ballast stiffness and damping, respectively.

By combining all the equations above, a standard matrix form of the governing equations of the system can be formulated and expressed as follows

$$\begin{cases} \boldsymbol{M_{engage}}\ddot{X}(t) + \boldsymbol{C_{engage}}\dot{X}(t) + \boldsymbol{K}X(t) = \boldsymbol{F}(t) & Engagement \\ \boldsymbol{M_{disengage}}\ddot{X}(t) + \boldsymbol{C_{disengage}}\dot{X}(t) + \boldsymbol{K}X(t) = \boldsymbol{F}(t) & Disengagement \end{cases} \tag{30}$$

where $\ddot{X}(t)$, $\dot{X}(t)$, and $X(t)$ are the generalized acceleration, velocity and displacement vectors, respectively; $\boldsymbol{M_{engage}}$ and $\boldsymbol{M_{disengage}}$ are generalized mass matrices during engagement and disengagement, respectively; $\boldsymbol{C_{engage}}$ and $\boldsymbol{C_{disengage}}$ are generalized damping matrices during engagement and disengagement, respectively; $\boldsymbol{K}$ is generalized stiffness matrices, which keeps unchanged during the switching of engagement and disengagement and $\boldsymbol{F}(t)$ is the corresponding force, which contains the eight moving load f_1~ f_8 and the generalized modal forces.

3.4. Simulation of energy harvesting performance

Simulation has been conducted using the developed comprehensive train-track-harvester model. Since the formulated matrices have a very large size and equations are coupled with the nonlinearity of the engagement and disengagement characteristics, the conventional direct time integration method is inefficient and computationally expensive. An improved fast explicit integration algorithm, proposed by *Zhai* [33,34], has been adopted in this paper to solve the governing equations, which can be expressed as follows

$$\{X\}_{n+1} = \{X\}_n + \{V\}_n\Delta t + \left(\frac{1}{2} + \psi\right)\{A\}_n\Delta t^2 - \psi\{A\}_{n-1}\Delta t^2 \tag{31}$$

$$\{V\}_{n+1} = \{V\}_n + (1 + \varphi)\{A\}_n\Delta t - \varphi\{A\}_{n-1}\Delta t \tag{32}$$

where Δt is the time step. The maximum time step size for the freight train-track system is found to be 5×10^{-5} s [33,34]. X, V and A are modal displacement, velocity and acceleration, respectively. $n + 1$, n

Table 2
Simulation parameters.

Parameters	Description	Value
f_0	Static moving load	105 kN(@30 km/h)
m_r	Rail mass per meter	51.5 kg/m
EI	Elastic modulus of rail	4×10^6
K_{pk}	Rail-pad stiffness	20 MN/m
C_{pk}	Rail-pad damping	21.8 KNs/m
K_{bk}	Ballast stiffness	10 MN/m
C_{pk}	Ballast damping	21.8 KNs/m
m_{sk}	Sleeper mass	125.5 kg
l_s	Sleeper spacing	0.545 m
l	Rail length	139.52 m
V_0	Train speed	20~80 km/h

and $n-1$ represent every three adjacent time step. φ and ψ are integration parameters, which are both chosen as 0.5 in the simulation.

The parameters of the simulation are listed in Table 2. A two-unit rapid transit train with 4 wheelsets per unit was selected in the simulation, and the results of the two prototypes are shown in Fig. 6. Fig. 6(a) illustrates the simulated track displacement (at the harvester installation point) at 20 km/h train speed, single-phase voltage and single-phase power with an 8 Ohm resistive load. It should be noted that while the train passes by, the track deflects down and up when every wheelset approaches and leaves, exciting the harvester to produce energy twice for a single wheel. The first four wheelsets of the first rapid transit unit contribute the first four displacement valleys, while the last four displacement valleys come from the four wheelsets of the second rapid transit unit as shown in Fig. 6(a). Results with similar shapes are also expected for the freight trains cases, but since freight train track deflection will have larger amplitudes and frequencies due to higher train speed and load, higher power output will be achieved.

Fig. 6(b) and 6(c) show the simulated average power versus different train speeds and external resistive loads for two different prototypes. The dash lines represent the results that consider the moving loads as constants, which means that the wheel-rail force remains unchanged when the train moves at different speeds. The solid lines represent the results that consider the moving loads as speed-dependent ones, in other words, the wheel-rail vertical contact force will be larger when the train runs faster due to the rail irregularity and train dynamics [35,36], which is much closer to the real case. As the train speed increases, the simulated power could be larger and the average power is 5–10 W for prototype 1 and 20–30 W for prototype 2 at 60 km/h, which

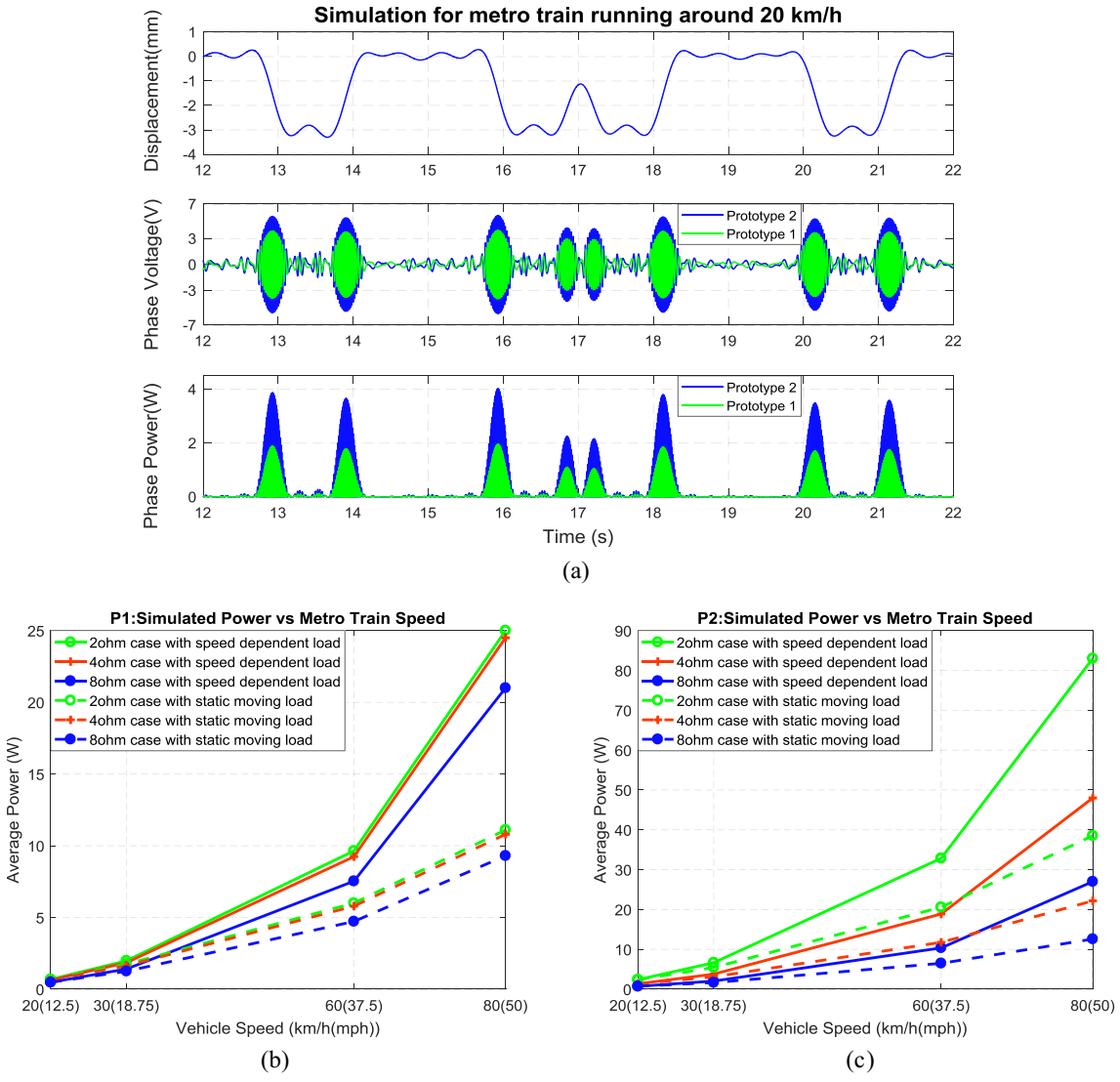

Fig. 6. (a) Simulation results with an 8 Ohm Wye shape resistive load when rapid transit speed is 20 km/h: prototype 1 and prototype 2. Simulated average power under different train speed with different resistive loads: the solid line is the simulation results with speed-dependent moving load and the dashed line is the simulation result with static moving load: (b) prototype 1; (c) prototype 2.

could be an adequate energy source for most of the smart electronic devices.

3.5. Dynamic influence on the railway track and vehicle

The dynamic influence of the energy harvester to the railway track and vehicle is very important to the train operation safety. Fig. 7(a) shows the simulated vertical displacement comparison of railway track with and without energy harvesters: the black solid line, representing the track displacement without any harvester beneath, matches very well with the red dash line, representing the track displacement with Harvester 1 beneath, and green dot line, representing the track displacement with Harvester 2, when the rapid transit train runs 20 km/h and harvester connected with a 2 Ohm Wye shape external resistive load. Fig. 7(b) shows the simulated displacement RMS differences between the track with the harvester 1 and 2 beneath (connected with 2 Ohm Wye shape external resistive load) and the track without energy harvester beneath, at different vehicle speeds. Compared with harvester 1, harvester 2 has a larger RMS difference; this is because harvester 2 provides more damping to the train-track system and recovers more power from the system. This difference increases when the rapid transit train runs faster; however, the overall RMS difference is still very small even at the maximum operation speed of 80 km/h for the rapid transit train. In other words, the influence of integrating the harvester to the railway track is so small that it will not affect the track and train dynamics, which will not bring any safety issue to the train operation.

4. Lab bench test and analysis

4.1. Experiment setup

Fig. 8 shows the in-lab bench test setup for the proposed ball screw based energy harvester. The ground plate was connected to the upper grip of the Instron hydraulic test machine through a T-shape adapter, and the input plate of the harvester was connected to the lower grip using an L-shape adapter and a connecting board. The lower grip could be driven by the hydraulic actuator and controlled by the built-in software and a 100 kN load cell together with an LVDT displacement sensor was used to measure the force and displacement during the test. A Wye shape resistive load with a 19:1 voltage divider was prototyped into a printed circuit board (PCB) which was connected to the generator of the harvester during the in-lab test. The voltage across the external resistor was measured and recorded by both Instron software and external dynamic analyzer (Spider 80) during each test. The ball screw harvester was tested with both sinusoidal excitation and measured track displacement excitation, and the corresponding energy harvesting performance will be evaluated in the following.

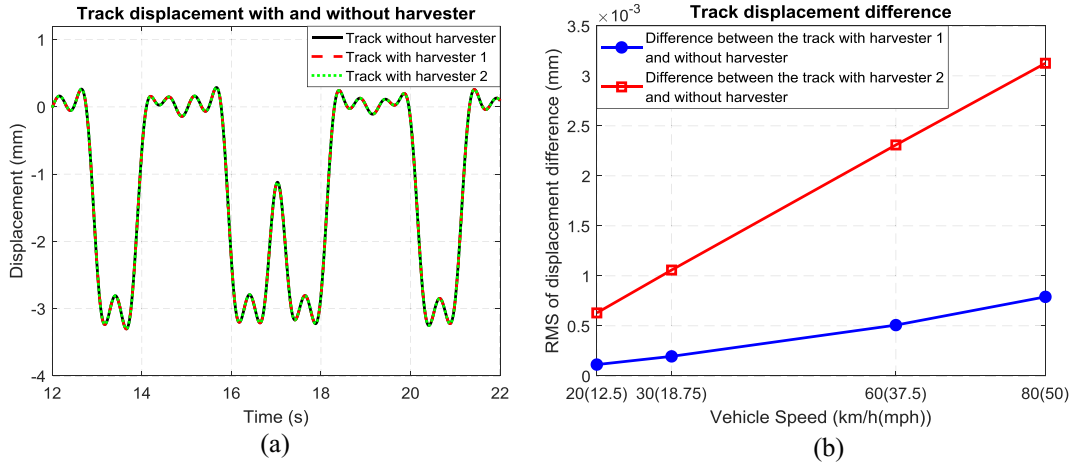

Fig. 7. Dynamic influence of the energy harvester to the track: (a) railway track vertical displacement due to the wheel-rail vertical force when the train runs at around 20 km/h: the black solid line represents the track displacement without any harvester beneath, the red dash line represents the track displacement with harvester 1 beneath connected with a 2 Ohms external resistive load and the green dot line represents the track displacement with harvester 2 beneath connected with a 2 Ohms external resistive load; (b) the displacement RMS differences between the tracks with the harvester 1 and harvester 2 beneath (connected with 2 Ohms external resistive load) and the tracks without the harvester beneath, at different vehicle speeds.

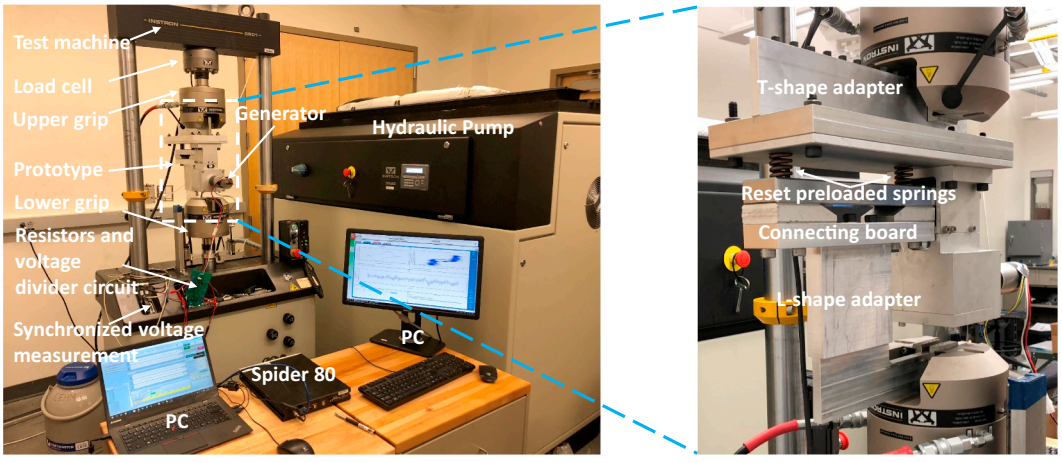

Fig. 8. In-lab experiment setup.

4.2. Harmonic excitation

A series of sinusoidal displacement excitations with different amplitudes and frequencies were input to the energy harvesters. During the test, the generator was observed to start to rotate at ± 0.2 mm vibration amplitude, which indicates the overall prototype has a relatively small backlash and a high sensitivity towards the environmental vibration. The average power of the prototype 1 and prototype 2 under 1 Hz excitation frequency, 1–3 mm amplitude with different resistive loads are summarized in Table 3, as well as the electrical damping coefficient for the two prototypes. As we can see, with the same external resistive load, the damping of prototype 2 is much larger than prototype 1, because the two prototypes use different generators and gearhead amplification ratios. The average power of the two prototypes in the harmonic test becomes larger when the vibration amplitude increases since the average input speed is increased. Meanwhile, the average power becomes larger when the external resistive load decreases, and this is because the electrical damping coefficient becomes larger, which means more mechanical energy could be converted to the electrical energy at the same time period. The energy harvesting output power of the prototype 2 is higher than that of the prototype 1 because the multiplication of speed constant of the generator 2 and its corresponding gearhead amplification ratio is larger.

Fig. 9 shows the simulated and measured phase voltage and power of the ball screw harvester 2 with an Wye shape external resistive load of 8 Ohms, under amplitude of ± 3 mm and frequency of 2 Hz. The phase voltage subplot illustrates that the generator is still rotating when the displacement reaches the peak or valley, showing the harvester disengages at that moment and generator rotates freely with viscous damping. An average power of 26.61 W was achieved during this test and simulation results matched well with experimental results.

4.3. Measured freight train track vibration

A freight train track displacement previously measured in Transportation Technology Center, Inc. (TTCI) [29] was used as input to the harvester, to further investigate the performance of the proposed energy harvester. Fig. 10 shows the phase voltage and power of ball screw based energy harvester prototype 2 connected with 8 Ohm Wye shape resistive load under the measured displacement at the speed of 64 km/h (40 mph), and a peak power of 114.98 W at the single phase and an average power of 17.50 W at three phases were achieved during the experiment. Simulation results by using harvester model with measured track displacement inputs are also illustrated in Fig. 10. As we can see, the simulation results match well with the experiment results, which validates the effectiveness of the harvester model. Table 4 illustrates the damping coefficient and energy harvesting performance of the prototype 1 and prototype 2. It should be noted that, for both of the two prototypes, when the external resistive load is reduced, the damping and average power will be increased. As we know, if the rotational speed of a generator is constant, the output power on the external resistor will be the maximum when the external resistive load approaches the internal resistive load. During the in-lab test, the displacement input can be regarded as constant, and prototype 1 has a 2.28 Ohm sterminal resistance phase to phase, while prototype 2 has a 0.284 Ohm terminal resistance phase to phase. Therefore, for prototype 1, when the external resistive load is 2 Ohm, the output power should be around the maximum point, however, for prototype 2, if the external resistive load is reduced continuously, ideally the output power will be even larger. From Table 4, when the external resistive load of prototype 2 decreases from 4 Ohm to 2 Ohm, the power should increase significantly, however, the output power remains almost the same. One possible reason for this abnormal phenomenon is that the resisting

Table 3
Test results under harmonic excitations with a 1 Hz frequency.

Prototype 1	Damping	1 mm	2 mm	3 mm	Prototype 2	Damping	1 mm	2 mm	3 mm
2 ohm	67,762 Ns/m	0.8 W	3.2 W	7.1 W	2 ohm	168,640 Ns/m	0.9 W	6.5 W	17.7 W
4 ohm	46,182 Ns/m	0.5 W	2.0 W	4.6 W	4 ohm	89,908 Ns/m	0.8 W	4.9 W	12.3 W
8 ohm	28,212 Ns/m	0.3 W	1.40 W	3.0 W	8 ohm	46,495 Ns/m	0.5 W	3.0 W	7.3 W

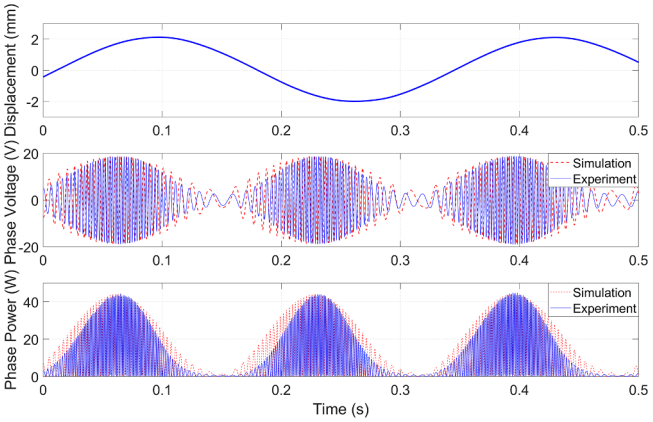

Fig. 9. Measured and simulated phase voltage and power of harvester prototype 2 under sinusoidal excitation with amplitude ± 2 mm and frequency 3 Hz. The harvester is connected with an 8 Ohm resistive loads in Wye shape and the average power of the total three phases is 26.61 W.

Fig. 10. Energy harvesting performance of the ball screw based harvester under measured freight train (running at 64 km/h) track displacement with 8 Ohm resistive loads in a Wye shape. The peak power in a single phase is **114.98 W** and the average power in all three phases are **17.50 W**.

Table 4
Energy harvesting performance under freight train track deflection for ball screw based track energy harvesters.

Prototype 1	Damping	Avg. Power	Prototype 2	Damping	Avg. Power
2 ohm	67,762 Ns/m	20.10 W	2 ohm	168,640 Ns/m	**23.54 W**
4 ohm	46,182 Ns/m	17.60 W	4 ohm	89,908 Ns/m	23.17 W
8 ohm	28,212 Ns/m	11.40 W	8 ohm	46,495 Ns/m	17.50 W

torque from the generator becomes larger when the external resistive load is reduced. Therefore, the clutches embedded in the large bevel gears reach their torque limit and slip, which reduces the rotational transmission from the shaft to the bevel gears, resulting in less output power than what it is expected when decreasing the external resistive load.

4.4. Rapid transit track vibration

Rapid transit track deflections were measured with the vehicle running at different speeds on a rapid transit test line located at Tongji University campus, and harvesters were tested in lab with these measured track displacements. During the test, the preload of the reset springs was set to be around 2500 N. As shown in Fig. 11(a), a single phase peak power of 13.36 W and a three-phase average power of 1.58 W were obtained from prototype 2 under rapid transit track displacement (measured when rapid transit runs at 30 km/h) with 8 Ohm resistive loads in Wye shape. The force measured in the test and obtained in the simulation is the force from the upper grip to the harvester base plate, and negative force means that the upper grip is continuously supporting or pushing the base plate. As we can see, the simulation results match well with the experiment results, which validates the effectiveness of the harvester model. Fig. 11(b) shows single-phase peak power and three-phase average power of both prototype 1 and prototype 2 using the measured displacement with different resistive loads. 20 km/h and 30 km/h cases used real measured displacement as excitation input, and 60 km/h and 80 km/h cases used measured displacement with a compressed time, which means that the peak displacement will be kept as the same as low-speed case, while the time has been compressed to simulate higher train speed. As shown in Fig. 11(b), the dash lines are the output power results for prototype 1 and the solid lines are for the prototype 2. The peak power and average power increase when the simulated train speed increases, and the average power at simulated 60 km/h and 80 km/h cases could achieve around 5 W and 9 W for prototype 1 and 8 W and 11 W for prototype 2, which will be adequate for many trackside electronic applications and devices. The in-lab rapid transit track displacement track test results for prototype 1 have the same trend with the simulation results in Fig. 6 (c), and they match well with each other; however, for prototype 2, the test results and simulation results don't match well, especially when the external resistive load is small, such as the 2 Ohm case and 1 Ohm case. The reason for the mismatches at lower external resistor cases can be the resisting torque on the one-way clutch is larger than its limits, so that the clutch slipped during the experiment and cannot transmit the motion to the bevel gears, therefore the output rotational speed of the generator could not be fast enough as it is expected, and the output power will not be as high as we expected or even lower at a smaller resistor case compared with a higher resistive load.

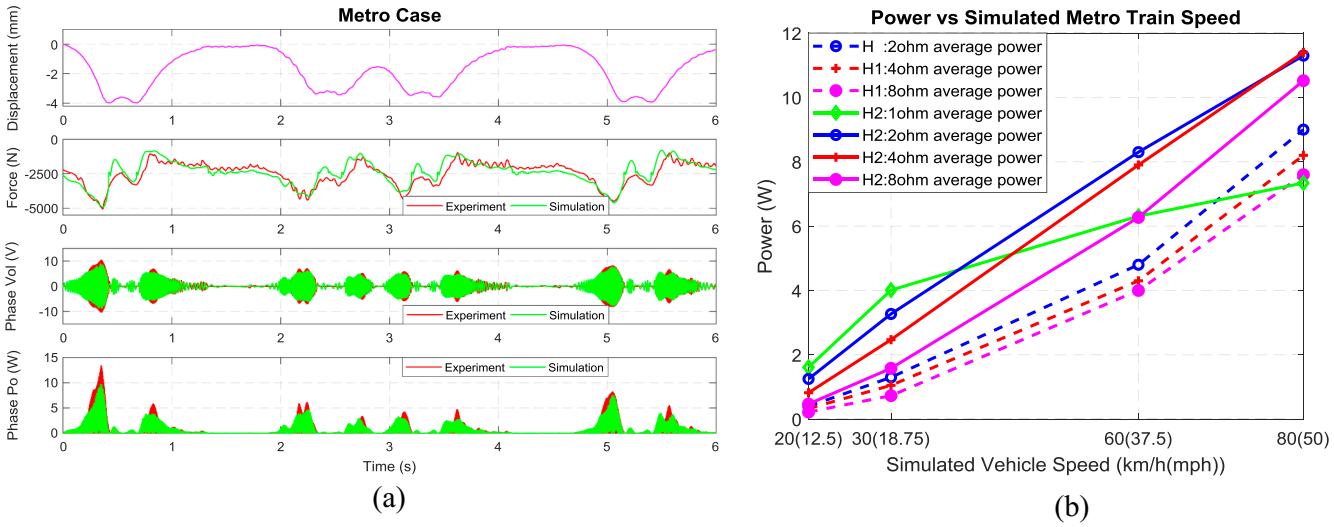

Fig. 11. (a) in-lab test and simulation results of prototype 2 under rapid transit train (running at around 30 km/h) track displacement with an 8 Ohm resistive loads in Wye shape: single phase peak power in lab test is **13.36 W** and three-phase average power in lab test is **1.58 W**; (b) three-phase average power of both ball screw harvester prototype 1 and prototype 2 under simulated track displacement input using the measured displacement with different external resistive loads: the dash lines are for prototype 1 and the solid lines are for the prototype 2.

5. Field test and discussion

5.1. Test setup

Field test was carried out on a rapid transit test track located at Tongji University campus in Shanghai to validate the energy harvesting performance. Prototype 1 and 2 have been tested respectively. Fig. 12 shows the experimental setup. The harvester was placed between two wooden sleepers on a ballast bed. The long input plate of the harvester was mounted rigidly under the test railway track. The ballast below the harvester prototype was cleared for fitting 4 jacks which supported the base plate of the harvester and provide a preload for the harvester input plate by compressing the reset springs. During the test, a two-unit rapid transit ran at around 20 km/h and 30 km/h on the ballast test line repeatedly. Two laser displacement sensors were used to measure the rail motion and harvester motion. Different Wye shape resistive loads were connected to the harvester during tests. A data acquisition system was employed to collect the displacement and voltage data and record the condition of harvester and rail when the rapid transit trains passed by.

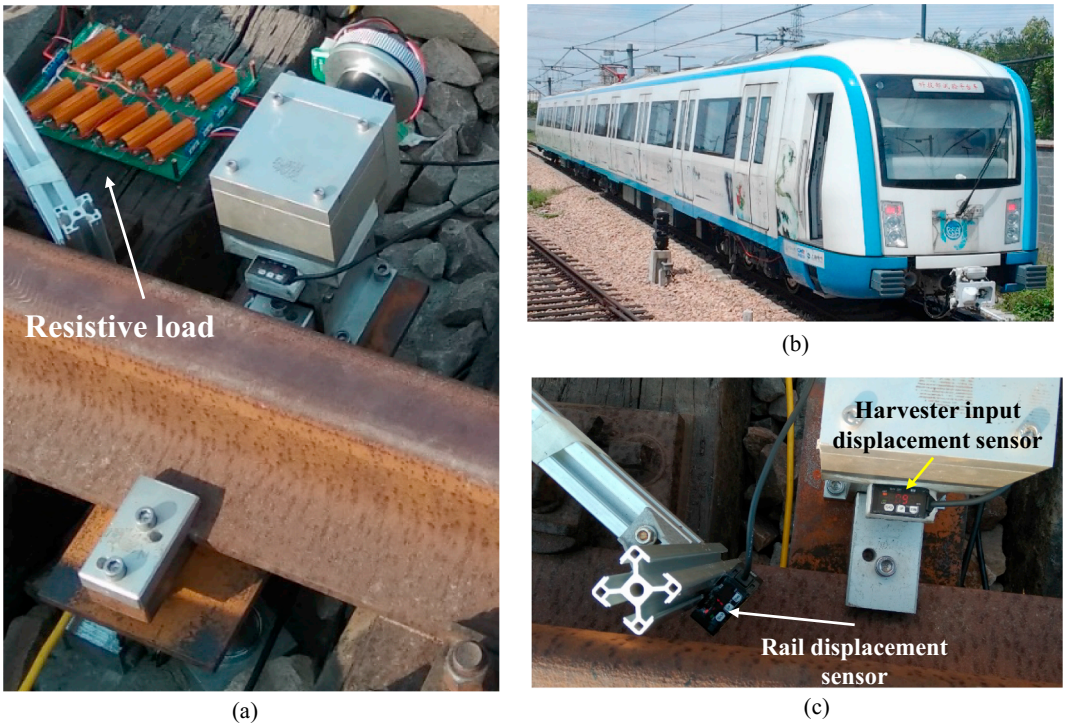

Fig. 12. In field test setup: (a) Harvester prototype 1 was clamped on the railway track and positioned between two adjacent sleepers. (b) A two-unit Type A rapid transit ran with a speed of 20–30 km/h; (c) Two laser displacement sensors measured the railway track displacement and harvester input displacement, respectively.

5.2. Results and discussion

Fig. 13(a) shows the measured and simulated rail displacements, harvester input displacements and measured single-phase voltage over an 8 Ohm Wye shape external resistor at the train speed of 20 km/h. The input displacement of the harvester followed closely with the rail displacement. A peak power of 1.64 W and an average power of 0.27 W were achieved.

Fig. 13(b) shows the measured and simulated rail displacements, harvester input displacement and measured single-phase voltage of generator of prototype 1 with a 2 Ohm Wye shape external resistor when the trains passed with 30 km/h speed. A peak power of 7.8 W and an average power of 1.12 W were achieved during this 8-second test. It is noted that during the test, the harvester displacement followed well when railway track moved downward, but not well when the track moved back. As a result, the voltage during the rail deflected was large, while was relatively small when the railway track restored. Possible reasons for this problem are as follows: (1) the spring force is not large enough, especially at a small resistive load or a large speed. When the vehicle speed increased, the track deflection speed and acceleration became large, so the damping force and the inertia force became larger, which means that the harvester needed larger spring force to push the base plate to keep still on the ground; (2) during the reciprocating test, ballast below the harvester became loose so that the preload provided by the reset spring was smaller than that of the first several tests. Inadequate spring force resulted in the base plate being separated with the rail foundation so the restored speed of harvester was smaller, therefore, the voltage of the generator became smaller when the track restored back.

Table 5 summarizes the field test results of the prototype 2. A maximum average power of 2.24 W was achieved with 8 Ohm Wye shape resistive load at a rapid transit speed of 30 km/h. This energy could be stored in a battery through self-designed or commercial battery charging circuits and used to power different trackside electrical devices, such as signal lights, track switches, hot box detectors, rail health monitoring systems, and wireless communication modules, which could potentially increase the safety of train operation. The power outputs are expected to be larger with smaller resistive loads than that of 8 Ohm but ended up with a lower power due to possible inadequate spring forces and clutch slippage, which has been discussed above in this subsection and subsection *4.4*. More power could be expected by choosing a higher limit one-way clutch, increasing the reset spring stiffness and refining the installation condition.

Table 5
Field test results summary for Prototype 2.

	Resistor		
Speed	8 Ohm	4 Ohm	2 Ohm
20 km/h (12.4 mph)	1.16 W	1.24 W	1.36 W
30 km/h (18.6 mph)	**2.24 W**	2.04 W	1.48 W

6. Conclusions

In this paper, a novel ball screw based railway track energy harvester with mechanical motion rectifier mechanism was designed, modeled and tested. Due to the nonlinear characteristics induced by the one-way clutches in the mechanical motion rectification (MMR) mechanism, the proposed energy harvester could convert the bi-directional track vibration into unidirectional rotation of the generator, which significantly improves the motion transmission by reducing the impact forces. A comprehensive model considering the coupled dynamic behaviors of the train, railway track and harvester was developed and validated. It is shown that the proposed ball screw based energy harvester acts as a fixed inerter in parallel with pre-compressed springs and an adjustable damper tuned by external resistive load of the generator, when the one-way clutch is in engagement. When both one-way clutches disengage from the bevel gears, the energy harvester behaves as pre-compressed springs only, and the inertia of the generator drives the generator itself continuously to produce electricity. This piece-wise mass-spring-damper of the single freedom harvester is integrated into the train-track model and the performance of the harvester at different train speeds can be predicted by the model.

The in-lab and field tests were conducted to further validate the dynamic characteristics and evaluate the performance of the proposed energy harvester. The harvester could effectively work under a very small input with the amplitude of ±0.2 mm, which shows that the proposed harvester has an improved sensitivity to the environment vibrations. Field test results showed that an average power of 1.12 W and 2.24 W were achieved for prototype 1 and 2 respectively at 30 km/

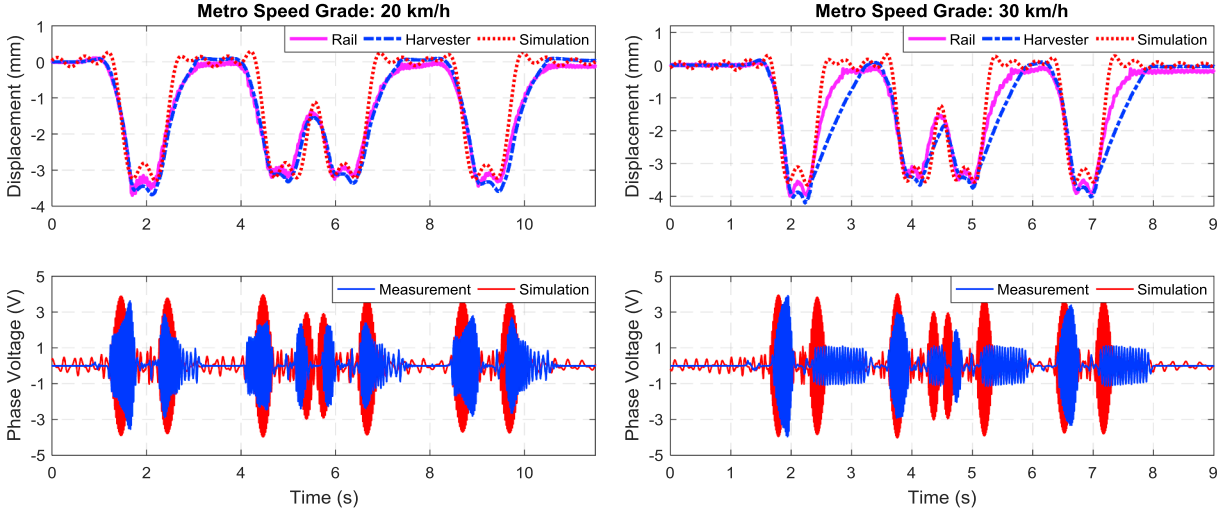

Fig. 13. Measured and simulated rail and harvester displacements and measured voltages at different vehicle speeds: (a) rapid transit train speed is 20 km/h and the external resistive load is 8 Ohm. The average power obtained in the test is 0.27 W; (b) rapid transit speed is 30 km/h and the external resistive load is 2 Ohm. An average 1.12 W was achieved in the test.

h rapid transit speed. More power could be obtianed by choosing a higher limit one-way clutch, increasing the reset spring stiffness and refining the installation condition.

Acknowledgment

This research is partially supported by Commonwealth Research Commercialization Fund (Grant No. MF16-003-En), National Natural Science Foundation of China (Grant No. 51728503), and State Key Laboratory of Traction Power at Southwest Jiao Tong University Open Grant (Grant No. TPL 1808). We would like to thank Dr. Mehdi Ahmadian for the discussions, and Campbell Neighborgall and Sijing Guo for their help to improve the writing.

References

[1] Tai W-C, Liu M, Yuan Y, Zuo L. On improvement of the frequency bandwidth of nonlinear vibration energy harvesters using a mechanical motion rectifier. J Vib Acoust 2018;140:051008–51011.
[2] Zhou S, Zuo L. Nonlinear dynamic analysis of asymmetric tristable energy harvesters for enhanced energy harvesting. Commun Nonlinear Sci Numer Simul 2018;61:271–84.
[3] Viet NV, Xie XD, Liew KM, Banthia N, Wang Q. Energy harvesting from ocean waves by a floating energy harvester. Energy 2016;112:1219–26.
[4] Younesian D, Alam M-R. Multi-stable mechanisms for high-efficiency and broadband ocean wave energy harvesting. Appl Energy 2017;197:292–302.
[5] Zhou S, Wang J. Dual serial vortex-induced energy harvesting system for enhanced energy harvesting. AIP Adv 2018;8:075221.
[6] Zhang R, Wang X, Al Shami E, John S, Zuo L, Wang CH. A novel indirect-drive regenerative shock absorber for energy harvesting and comparison with a conventional direct-drive regenerative shock absorber. Appl Energy 2018;229:111–27.
[7] Bowen L, Vinolas J, Olazagoitia J, Otero JE. An innovative energy harvesting shock absorber system using cable transmission. IEEE/ASME Trans Mechatron 2019;99. 1-1. (Early Access).
[8] Xiong H, Wang L. Piezoelectric energy harvester for public roadway: on-site installation and evaluation. Appl Energy 2016;174:101–7.
[9] Gao M, Wang Y, Wang Y, Wang P. Experimental investigation of non-linear multistable electromagnetic-induction energy harvesting mechanism by magnetic levitation oscillation. Appl Energy 2018;220:856–75.
[10] Coelho B, Hölscher P, Priest J, Powrie W, Barends F. An assessment of transition zone performance. Proc Instit Mech Eng Part F: J Rail Rapid Transit 2011;225(2):129–39. https://doi.org/10.1177/09544097JRRT389.
[11] Vorster J, Grabe H. Axle load and track deflection on a heavy haul line. Civil Eng: Magaz South Afric Instit Civil Eng 2010;18:44–9.
[12] Wischke M, Masur M, Kröner M, Woias P. Vibration harvesting in traffic tunnels to power wireless sensor nodes. Smart Mater Struct 2011;20:085014.
[13] Nelson CA, Platt SR, Albrecht D, Kamarajugadda V, Fateh M. Power harvesting for railroad track health monitoring using piezoelectric and inductive devices. Active and passive smart structures and integrated systems. International Society for Optics and Photonics; 2008. p. 69280R.
[14] Pourghodrat A, Nelson CA, Hansen SE, Kamarajugadda V, Platt SR. Power harvesting systems design for railroad safety. Proc Instit Mech Eng Part F: J Rail Rapid Transit 2014;228(5):504–21. https://doi.org/10.1177/0954409713482659.
[15] Tianchen Y, Jian Y, Ruigang S, Xiaowei L. Vibration energy harvesting system for railroad safety based on running vehicles. Smart Mater Struct 2014;23:125046.
[16] Wang J, Shi Z, Xiang H, Song G. Modeling on energy harvesting from a railway system using piezoelectric transducers. Smart Mater Struct 2015;24:105017.
[17] Nelson CA, Pourghodrat A, Fateh M. Energy harvesting from vertical deflection of railroad track using a hydraulic system for improving railroad track safety. ASME international mechanical engineering congress and exposition. 2011. p. 259–66.
[18] Gao M, Wang P, Cao Y, Chen R, Cai D. Design and verification of a rail-borne energy harvester for powering wireless sensor networks in the railway industry. IEEE Trans Intell Transp Syst 2017;18:1596–609.
[19] Gatti G, Brennan MJ, Tehrani MG, Thompson DJ. Harvesting energy from the vibration of a passing train using a single-degree-of-freedom oscillator. Mech Syst Sig Process 2016;66:785–92.
[20] Brennan MJ, Gatti GA. Harvesting energy from time-limited harmonic vibrations: mechanical considerations. J Vib Acoust 2017;139:051019.
[21] Pourghodrat A, Nelson CA, Phillips KJ, Fateh M. Improving an energy harvesting device for railroad safety applications. Active and passive smart structures and integrated systems. International Society for Optics and Photonics; 2011. p. 9.
[22] Pourghodrat A, Nelson CA. A system for generating electricity using the passage of train wheels for improving railroad track safety. ASME international design engineering technical conferences and computers and information in engineering conference. 2012. p. 1025–31.
[23] Wang JJ, Penamalli G, Zuo L. Electromagnetic energy harvesting from train induced railway track vibrations. Proceedings of IEEE/ASME international conference on mechatronic and embedded systems and applications. 2012. p. 29–34.
[24] Zhang X, Zhang Z, Pan H, Salman W, Yuan Y, Liu Y. A portable high-efficiency electromagnetic energy harvesting system using supercapacitors for renewable energy applications in railroads. Energy Convers Manage 2016;118:287–94.
[25] Zhang X, Pan H, Qi L, Zhang Z, Yuan Y, Liu Y. A renewable energy harvesting system using a mechanical vibration rectifier (MVR) for railroads. Appl Energy 2017;204:1535–43.
[26] Wang J, Lin T, Zuo L. High efficiency electromagnetic energy harvester for railroad application. ASME 2013 international design engineering technical conferences and computers and information in engineering conference. 2013. p. V004T08A37-VT08A37.2013.
[27] Lin T, Wang JJ, Zuo L. Efficient electromagnetic energy harvester for railroad transportation. Mechatronics 2018;53:277–86.
[28] Lin T, Pan Y, Zuo L. Dynamics modeling of train-track-harvester system and in-field testing of railroad energy harvester. ASME 2016 dynamic systems and control conference. 2016. p. V001T13A-VT13A.
[29] Lin T, Pan Y, Chen S, Zuo L. Modeling and field testing of an electromagnetic energy harvester for rail tracks with anchorless mounting. Appl Energy 2018;213:219–26.
[30] Li Z, Zuo L, Luhrs G, Lin L, Qin Y-x. Electromagnetic energy-harvesting shock absorbers: design, modeling, and road tests. IEEE Trans Veh Technol 2013;62:1065–74.
[31] Liu Y, Xu L, Zuo L. Design, modeling, lab, and field tests of a mechanical-motion-rectifier-based energy harvester using a ball-screw mechanism. IEEE/ASME Trans Mechatron 2017;22:1933–43.
[32] Li Z, Zuo L, Kuang J, Luhrs G. Energy-harvesting shock absorber with a mechanical motion rectifier. Smart Mater Struct 2013;22:025008.
[33] Zhai W, Cai Z. Dynamic interaction between a lumped mass vehicle and a discretely supported continuous rail track. Comput Struct 1997;63:987–97.
[34] Zhai W. Vehicle-track coupling dynamics. Beijing, People's Republic of China: China Railway Press; 2007.
[35] Li D, Selig ET. Method for railroad track foundation design. II: applications. J Geotech Geoenviron Eng 1998;124:323–9.
[36] Van Dyk BJ, Edwards JR, Dersch MS, Ruppert Jr CJ, Barkan CP. Evaluation of dynamic and impact wheel load factors and their application in design processes. Proc Instit Mech Eng Part F: J Rail Rapid Transit 2017;231(1):33–43. https://doi.org/10.1177/0954409715619454.